Electron and magneto-optical properties of half-metallic ferromagnets and uranium monochalcogenide

1991 J. Phys.: Condens. Matter 3 6363

(http://iopscience.iop.org/0953-8984/3/33/014)

J. Phys.: Condens. Matter 3 (1991) 6363–6374. Printed in the UK

Electron and magneto-optical properties of half-metallic ferromagnets and uranium monochalcogenide

S V Halilov† and E T Kulatov‡

† Kurchatov Institute of Atomic Energy, Academican Kurchatov Square, Moscow 123182, USSR

‡ General Physics Institute, Vavilov Str. 38, Moscow 117942, USSR

Received 3 January 1991, in final form 25 April 1991

Abstract. Within the density-functional theory, including its local spin-density approximation, the fully relativistic calculations of electron, optical and magneto-optical spectra in some half-metallic ferromagnets and uranium monochalcogenide have been performed. An increase in the magneto-optical Kerr effect in half-metallic magnets is closely related to such factors as the spin–orbit exchange splittings and the plasma frequency. At the same time in the usual ferromagnets the peculiarities of band structure lead to anomalies in the conductivity tensor at energies close to the spin–orbit splitting.

1. Introduction

The experimental finding of the huge polar magneto-optical Kerr effect (MOKE) in PtMnSb (van Engen *et al* 1983) has inspired renewed theoretical interest in the study of electron and optical properties of similar compounds. A band-structure calculation for NiMnSb (de Groot *et al* 1983) indicated the existence of a new class of materials called half-metallic ferromagnets (HMFS). This theoretical study yields the interesting result that NiMnSb is metal for majority, or spin-up, electrons but exhibits a semiconductor-type gap for minority, or spin-down, electrons. CoMnSn (Kuebler 1984), FeMnSb (de Groot *et al* 1986), CrO_2 (Schwarz 1986), Fe_3O_4 (Yanase and Siratori 1984) and a number of other compounds have been assigned to the HMFS on the basis of band calculations. This raises the question of why, of all the known HMFS, PtMnSb possesses the greatest MOKE.

The sharp increase in MOKE in PtMnSb compared with NiMnSb is ascribed to the different locations of the Fermi level E_F relative to the bottom of the band gap in spin-down subband and the different spin–orbital interactions (SOIS) of these compounds (van Engen *et al* 1983). However, Kulatov and Mazin (1990) have shown that the position of E_F with respect to the gap cannot be reliably determined from the local-spin-density approximation (LSDA) calculations with the required accuracy. Again, in PtMnSn where the SOIS are almost identical with those in PtMnSb, MOKE is even less than in NiMnSb. Wijngaard *et al* (1989) concluded that the increase in MOKE in PtMnSb compared with NiMnSb is closely related to the different values of the scalar-relativistic effects in these substances.

0953-8984/91/336363 + 12 $03.50

2. Calculation method and energy dependence of the conductivity tensor $\sigma_{\alpha\beta}(\omega)$

Band-structure calculations for NiMnSb, PtMnSb and PtMnSn with a cubic structure of MgAgAs type with one embedded empty sphere and for US with a cubic NaCl structure have been performed using the linear muffin-tin orbital (LMTO) method (Andersen 1975). Exchange and correlation are treated in the LSDA. In the self-consistent calculations, scalar-relativistic effects (the mass–velocity and Darvin terms) and combined correction terms are included. The experimental lattice constants were used for all the above-mentioned compounds. In order to assess the dependence of the results on the choice of exchange–correlation energy function, we performed the calculations using four different approximations to the local exchange–correlation energy: the von Barth–Hedin (VBH) (1972) approximation, the Gunnarsson–Lundqvist (GL) (1976) approximation, the Janak–Moruzzi–Williams (JMW) (1975) approximation and Vosko–Wilk–Nussair (VWN) (1980) approximation. Incorporation of the SOI was achieved through the Kohn–Sham–Foldy–Wouthuysen equations (Itzykson and Zuber 1980). One electron spectrum resulting from these procedures was used for calculation of the conductivity tensor in accordance with the Kubo (1957) formula for the linear response functions.

Matrix elements of the dipole transitions were calculated directly from the LMTO eigenfunctions using a scheme derived by Uspenski *et al* (1983). It is known that a general form of the conductivity tensor is determined by the magnetic space group of crystal and so it depends on the orientation of magnetization (Kleiner 1966, Halilov and Uspenski 1990). For simplicity we have considered only the case of a single direction ($\boldsymbol{M} \parallel [001]$), where of the non-diagonal components of the tensor $\sigma_{\alpha\beta}(\omega)$ there are only the odd components on $\boldsymbol{M}$, which describe the MOKE. For cubic crystal structures this allows to use the Argyres (1955) expression, which is valid at sufficiently high frequencies $\omega \gg 2\bar{\xi}/\hbar$ (where $2\bar{\xi}$ is the mean value of the spin–orbital splitting). This expression shows that the dissipative part $\mathrm{Im}[\sigma_{xy}(\omega)]$ is proportional to the difference between dissipative parts of diagonal components with opposite spins, i.e. $\mathrm{Im}[\sigma_{xy}(\omega)] = \alpha'\{\mathrm{Re}[\sigma^{\downarrow}_{xx}(\omega)] - \mathrm{Re}[\sigma^{\downarrow}_{xx}(\omega)]\} = \alpha\{\mathrm{Re}[\sigma^{\uparrow}_{xx}(\omega)] + \mathrm{Re}[\sigma^{\downarrow}_{xx}(\omega)]\}$ ($\mathrm{Re}\,\sigma^{s}_{xx}(\omega)$] is due to the interband transitions with spin s (s = $\uparrow$, $\downarrow$) (Halilov and Uspenski 1990). The proportional coefficients $\alpha' \sim (\bar{\xi}/\Delta\bar{E})$ and $\alpha \sim (\bar{\xi}/\Delta\bar{E})(\Delta n/n)$, where $\Delta\bar{E}$ is the mean distance between one-particle levels and $\Delta n/n = (n^{\uparrow} - n^{\downarrow})/n$ is the relative magnetization.

At photon energies $\hbar\omega \simeq 2\bar{\xi}$ the hybridization of bands with opposite spins near E_F plays an important part in formation of the conductivity tensor $\sigma_{\alpha\beta}(\omega)$. Interband transitions in the region of proximity to the exchange-split bands with opposite spins ($m^{\uparrow}$) and ($m^{\downarrow}$) at E_F, if any, give at $\hbar\omega \simeq 2\sqrt{|\bar{\xi}|^2 + \Delta^2_{xc}}$ ($2\Delta_{xc}$ is the mean value of the exchange splitting) a sharp singularity in $\sigma_{\alpha\beta}(\omega)$ (Halilov and Uspenski 1988, 1990). The ratio $\mathrm{Im}(\sigma_{xy})/\mathrm{Re}(\sigma_{xx})$ at $\hbar\omega \simeq 2\sqrt{|\bar{\xi}|^2 + \Delta^2_{xc}}$ is found to be approximately $\bar{\xi}/\Delta\bar{E}$, i.e. under the described conditions a small quantity caused by the relative magnetization vanishes.

3. Characteristics of electron spectra

In XMnY compounds a large exchange splitting of the Mn d states leads to a situation in which the magnetic moment is localized mainly on the Mn site and the resulting Mn d bands tend to be polarized away from the Fermi energy. In some XMnY compounds the Fermi energy is situated inside the spin-down band gap. NiMnSb and PtMnSb are best suited to such systems even though, as noted above, the calculations indicate that

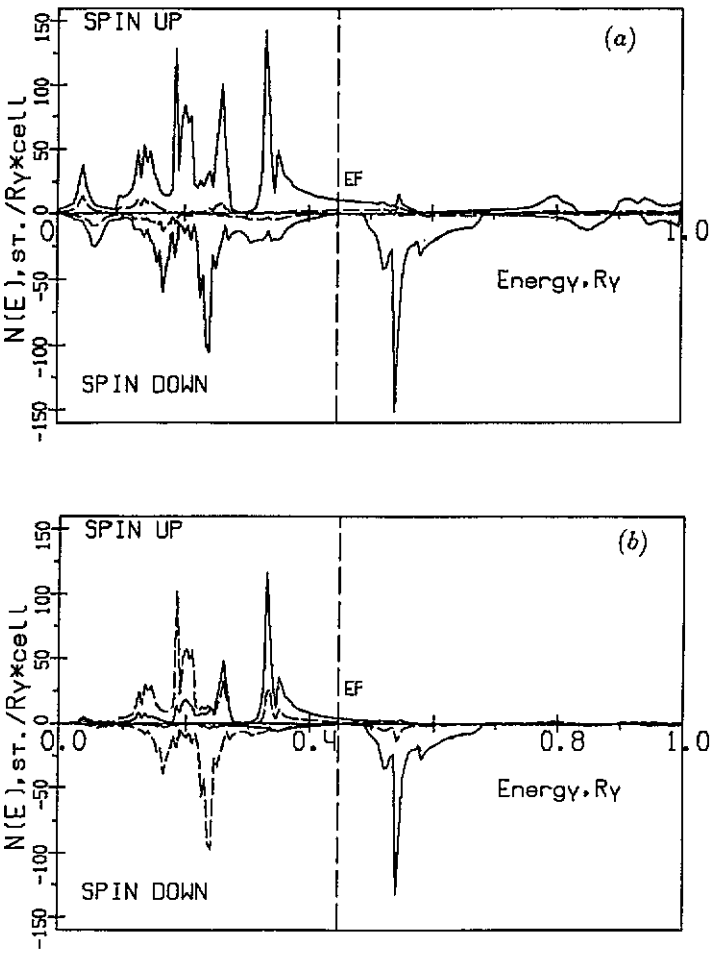

Figure 1. DOSs of NiMnSb: (*a*) ——, total DOS; – – – –, p DOS of Sb; (*b*), ——, d DOS of Mn; – – – –, d DOS of Ni.

the position of E_F in the gap is very sensitive to the exchange–correlation potential approximations. The calculations employing the VBH potential give the best results for the values of the magnetic moments. Let us take a brief look at those features of the band structure which play a dominant role in the formation of the conductivity tensor over the interval $0\ \text{eV} < \hbar\omega < 4\ \text{eV}$, where interband transitions are most intensive and the MOKE maxima are observed.

3.1. NiMnSb

Bands characterizing NiMnSb as a metal, i.e. crossing E_F, are mainly formed by $5s^{\uparrow}$ states of Sb and $(pd)^{\uparrow}$-hybridized states of Sb and Mn. The indirect gap in the spin-down subband is about 0.4 eV. The bands located just below the gap are composed mainly of the Sb $p^{\downarrow}$ states (threefold-degenerate level Γ_{15} split by the SOI). The Mn $d^{\downarrow}$ states are situated above the gap. The middle part of the valence band is composed mainly of Ni d states, which are almost not subjected to the exchange splitting (figure 1).

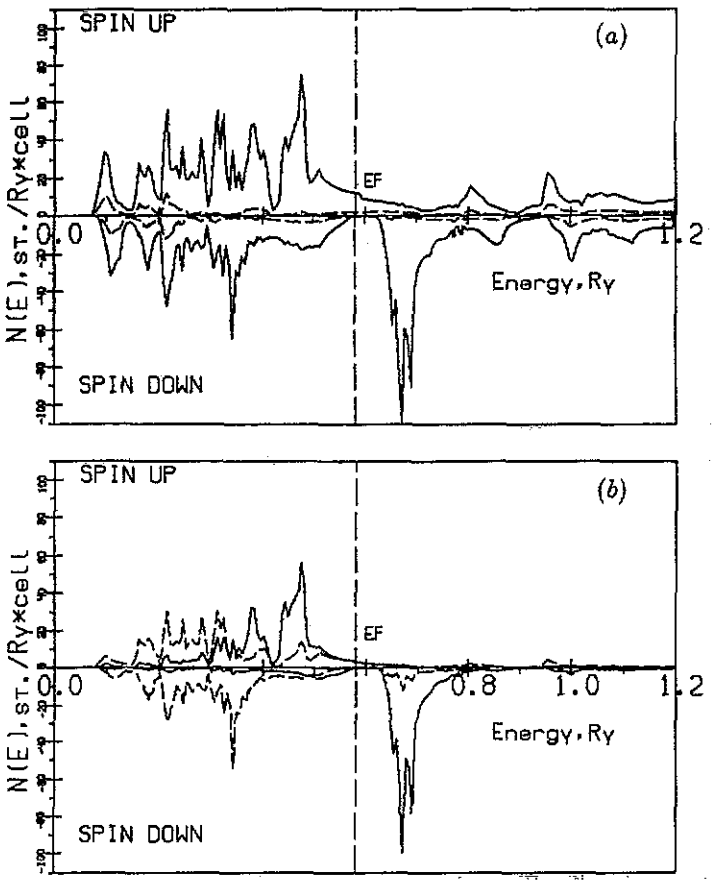

Figure 2. DOSs of PtMnSb: (*a*) ——, total DOS; – – – –, p DOS of Sb; (*b*) ——, d DOS of Mn; – – – –, d DOS of Pt.

3.2. PtMnSb

The changes in electron spectrum when Pt is substituted for Ni are due to an increase in the scalar-relativistic effects (Wijngaard *et al* 1989), which shift s states downwards in energy. The influence of SOI on the spectrum smoothes the Pt d density of states (DOS) through removal of the band degeneracies (figure 2).

3.3. PtMnSn

Substitution of Sn for Sb in PtMnSb causes a decrease in the number of valence electrons by one electron. In this case, E_F is lowered, the gap in the spin-down subband disappears (figure 3) and the magnetic moment is decreased (table 1).

3.4. US

Figure 4 shows the DOS functions in uranium monochalcogenide, where the MOKE is even larger than in PtMnSb. At the Fermi level there are the spin-up states as well as the spin-down states. The magnetism and conductivity in US are due to the U 5f states (the S p

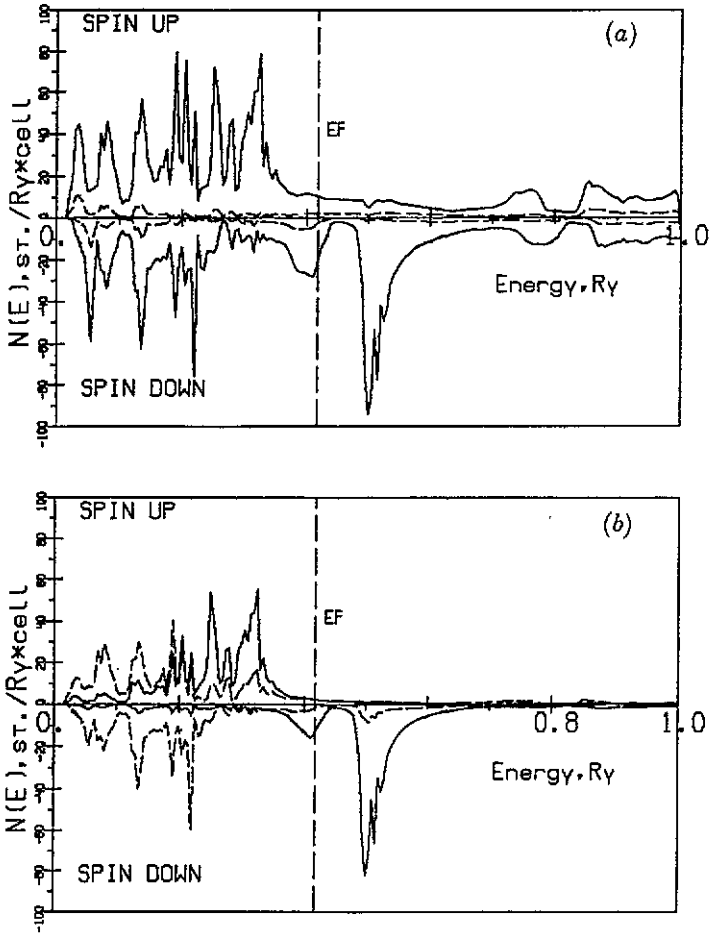

Figure 3. DOSs of PtMnSn: (*a*) ——, total DOS; – – – –, p DOS of Sn; (*b*) ——, d DOS of Mn; – – – –, d DOS of Pt.

Table 1. Calculated and observed magnetic moments.

	μ (μ_B)	
	Theory	Experiment
NiMnSb	4.00	3.85
PtMnSb	4.003	3.97
PtMnSn	3.51	3.42
US	2.37	1.70

states and the U f states are separated by 2.5 eV). As the spin–orbital and exchange splittings of the U f states are of the same order ($2\bar{\xi} \simeq 2\Delta_{xc}^{f} \simeq 1.5$ eV), the gap due to the SOI arises in both states $j = l + \frac{1}{2}$ and $j = l - \frac{1}{2}$. So the whole f band is divided into two subbands, separated by an interval of $2\bar{\xi}$. E_F crosses the lower subband.

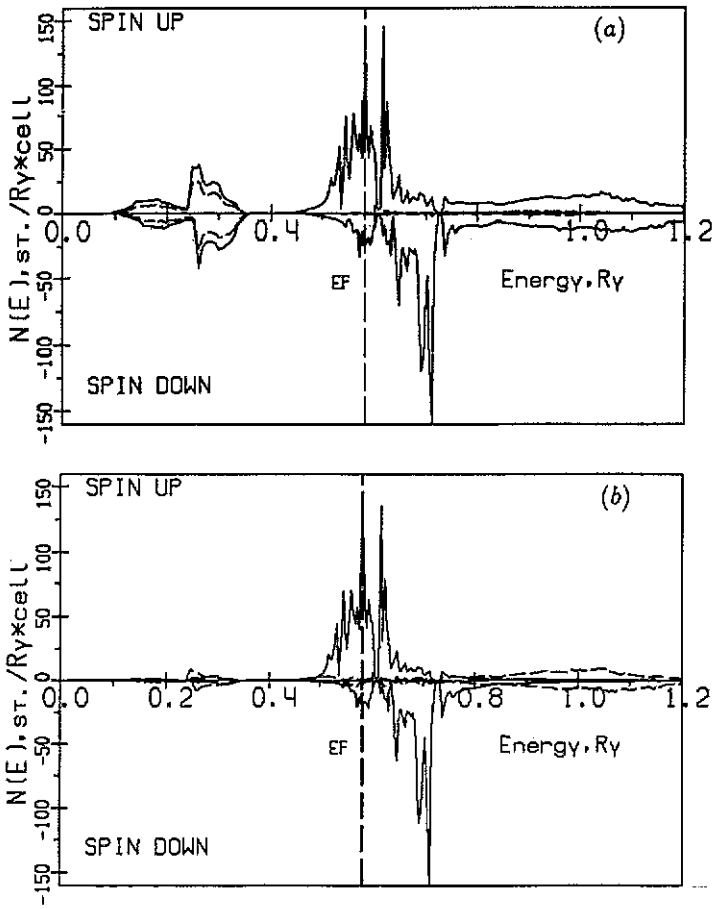

Figure 4. DOSs of US: (*a*) ——, total DOS; – – – –, p DOS of S; (*b*) ——, f DOS of U; – – – –, d DOS of U.

4. Magneto-optical spectra near the plasma frequency

The optical characteristics $\mathrm{Re}(\sigma_{xx})$ and $\mathrm{Im}(\sigma_{xy})$ for NiMnSb, PtMnSb and PtMnSn are shown in figures 5–7. The behaviour of $\mathrm{Im}(\sigma_{xy})$ is best understood if, in accordance with Halilov and Uspenski (1990), $\mathrm{Im}(\sigma_{xy})$ is represented as a difference of the optical conductivities with opposite spins, i.e. $\mathrm{Im}[\sigma_{xy}(\omega)] = \alpha'\{\mathrm{Re}[\sigma^{\uparrow}_{xx}(\omega)] - \mathrm{Re}[\sigma^{\downarrow}_{xx}(\omega)]\}$. Figure 5(*c*) shows $\mathrm{Re}[\sigma^{\uparrow}_{xx}(\omega)]$ and $\mathrm{Re}[\sigma^{\downarrow}_{xx}(\omega)]$ for NiMnSb. The total optical conductivity $\mathrm{Re}[\sigma_{xx}(\omega)] = \mathrm{Re}[\sigma^{\uparrow}_{xx}(\omega)] + \mathrm{Re}[\sigma^{\downarrow}_{xx}(\omega)]$ at energies $\hbar\omega \gg 2\bar{\xi}$. As one would expect, the interband part $\mathrm{Re}[\sigma^{\mathrm{inter}}_{xx}(\omega)]$ of the diagonal component for all Mn compounds under consideration are very similar—the main peaks of $\mathrm{Re}[\sigma_{xx}(\omega)]$ are located at 3.5 eV in NiMnSb and at 3.0 eV in PtMnSb(Sn) and are due to the $(\mathrm{p}^{\downarrow}_{\mathrm{Sb(Sn)}} \rightarrow \mathrm{d}^{\downarrow}_{\mathrm{Mn}})$ interband transitions. The principal differences in $\mathrm{Re}[\sigma_{xx}(\omega)]$ occur at low energies $\hbar\omega < 1.0$ eV by virtue of the great discrepancy between the intraband contributions; compare the specific electroresistivities $\rho_{\mathrm{NiMnSb}} \simeq 11$ mΩ cm, $\rho_{\mathrm{PtMnSb}} \simeq 13.5$ mΩ cm and $\rho_{\mathrm{PtMnSn}} \simeq 90$ mΩ cm at $T = 150$ K (Otto *et al* 1989), which correspond to the relaxation energies of intraband transitions in NiMnSb of about 0.47 eV and in PtMnSb of about

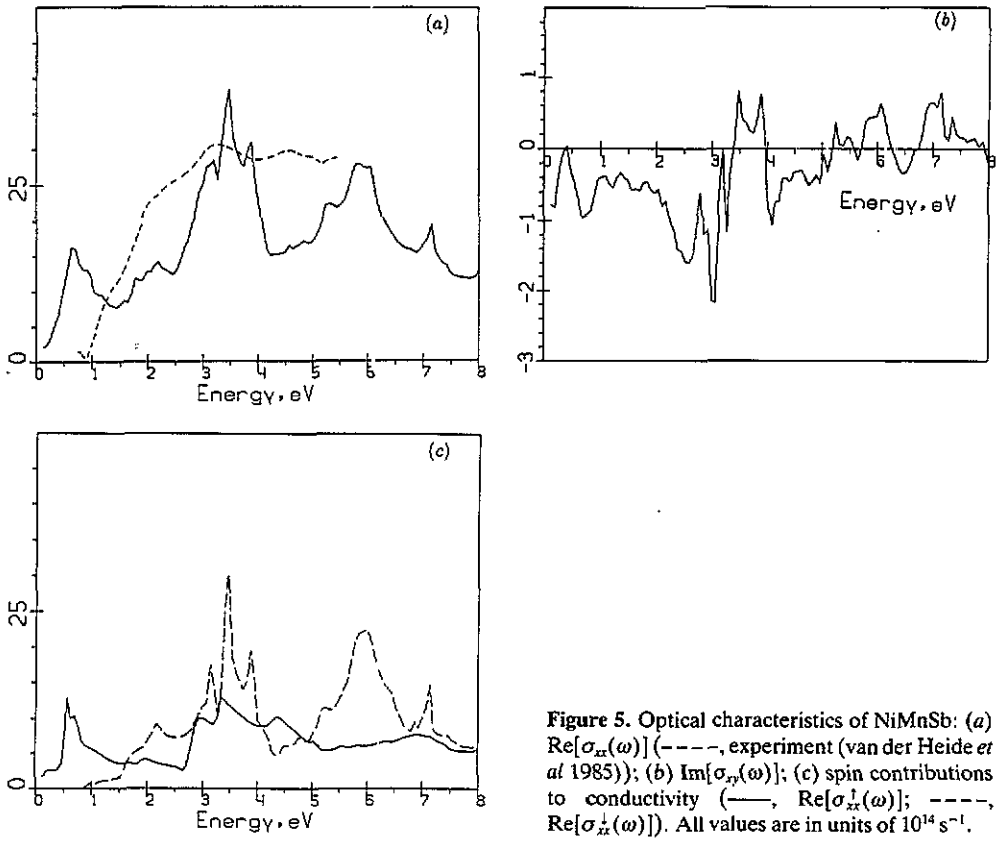

Figure 5. Optical characteristics of NiMnSb: (*a*) $\mathrm{Re}[\sigma_{xx}(\omega)]$ (– – – –, experiment (van der Heide *et al* 1985)); (*b*) $\mathrm{Im}[\sigma_{xy}(\omega)]$; (c) spin contributions to conductivity (——, $\mathrm{Re}[\sigma^{\uparrow}_{xx}(\omega)]$; – – – –, $\mathrm{Re}[\sigma^{\downarrow}_{xx}(\omega)]$). All values are in units of $10^{14}\,\mathrm{s}^{-1}$.

0.83 eV (van der Heide *et al* 1985). The intraband plasma energies are about 5–6 eV in the Mn compounds under consideration (van der Heide *et al* 1985), i.e. in Ni(Pt)MnSb the intraband contributions to the conductivity are four to five times smaller than in PtMnSn.

The behaviours of $\mathrm{Im}[\sigma_{xy}(\omega)]$, as the calculations imply, are also very similar. Our calculations of the Kerr angle do not confirm the observed enhancement of MOKE in PtMnSb. According to the experiments, $2\theta^{\mathrm{NiMnSb}}_{\mathrm{max}} \simeq 0.5°$ at $\hbar\omega \simeq 1.5$ eV, $2\theta^{\mathrm{PtMnSb}}_{\mathrm{max}} \simeq 2.5°$ at $\hbar\omega \simeq 1.7$ eV and $2\theta^{\mathrm{PtMnSn}}_{\mathrm{max}} \simeq 0.3°$ at $\hbar\omega \simeq 1.5$ eV. This raises the question of what is mainly responsible for the enhancement of MOKE. Argyres (1955) has shown that the relation between the Kerr angle and components of the tensor may be written as follows:

$$\theta(\omega) = \mathrm{Im}\{[n_+(\omega) - n_-(\omega)]/(n_+ n_- - 1)\} \tag{1}$$

where $n_{\pm}(\omega) = [\varepsilon_{xx}(\omega) \pm \mathrm{i}\varepsilon_{xy}(\omega)]^{1/2}$. In general, $\varepsilon_{\alpha\beta}(\omega)$ is the complex dielectric permeability, which may be represented as a sum of the dissipative ($\mathrm{Re}(\varepsilon_{xy})$ and $\mathrm{Im}(\varepsilon_{xx})$) and dispersional ($\mathrm{Re}(\varepsilon_{xx})$ and $\mathrm{Im}(\varepsilon_{xy})$) parts coupled by the Kramers–Kronig relations. It is easily seen from (1) that $\theta(\omega)$ will be increased at those energies when $n_+ n_- \simeq 1$.

Let us discuss this case in detail as opposed to Feil and Haas (1987) who oversimplified equation (1). The condition $n_+ n_- \simeq 1$, in essence, is valid at small values of $\varepsilon_{xx}(\omega)$, which corresponds to the existence of the plasma oscillations. However, account must be taken of the fact that the non-diagonal $\varepsilon_{xy}(\omega)$ and diagonal $\varepsilon_{xx}(\omega)$ components

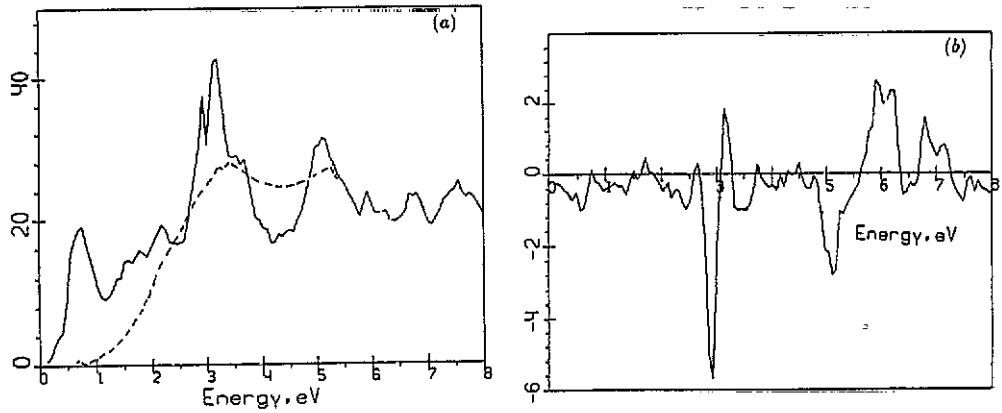

Figure 6. Optical characteristics of PtMnSb: (*a*) $\mathrm{Re}[\sigma_{xx}(\omega)]$ (----, experiment (van der Heide *et al* 1985)); (*b*) $\mathrm{Im}[\sigma_{xy}(\omega)]$. All values are in units of $10^{14}\,s^{-1}$.

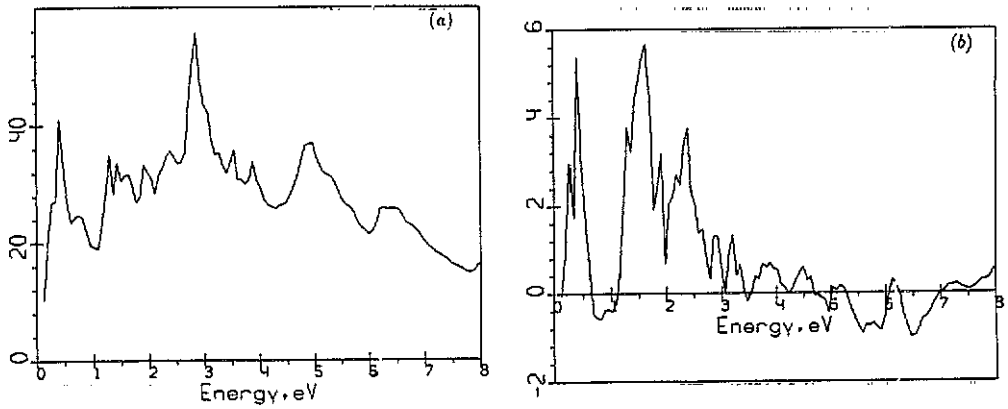

Figure 7. Optical characteristics of PtMnSn: (*a*) $\mathrm{Re}[\sigma_{xx}(\omega)]$; (*b*) $\mathrm{Im}[\sigma_{xy}(\omega)]$. All values are in units of $10^{14}\,s^{-1}$.

are formed by similar interband transitions. Roughly speaking, $\mathrm{Im}[\varepsilon_{xy}(\omega)] \simeq \alpha'\{\mathrm{Re}[\varepsilon^{\uparrow}_{xx}(\omega)] - \mathrm{Re}[\varepsilon^{\downarrow}_{xx}(\omega)]\}$, and in general the smallness of $\mathrm{Re}[\varepsilon_{xx}(\omega)]$ implies simultaneously the smallness of $\mathrm{Im}[\varepsilon_{xy}(\omega)]$. Because of this, to derive $\max[\theta(\omega_p)]$, where ω_p is the plasma frequency, one should take account of the listed proportions. Near the plasma resonance the dispersional parts $\mathrm{Re}[\varepsilon_{xx}(\omega_p)]$ and $\mathrm{Im}[\varepsilon_{xy}(\omega_p)]$ vanish; consequently $n_{\pm}(\omega_p) \simeq \sqrt{\varepsilon \pm i\gamma}$, $\varepsilon = \mathrm{Re}[\varepsilon_{xx}(\omega_p)]$, $\gamma = \mathrm{Im}[\varepsilon_{xy}(\omega_p)]$. By this means the Kerr angle at $\omega \simeq \omega_p$ may be written as

$$\theta(\omega \sim \omega_p) = \mathrm{Im}\left(\frac{\sqrt{\varepsilon + i\gamma} - \sqrt{\varepsilon - i\gamma}}{\sqrt{\varepsilon^2 + \gamma^2} - 1}\right) \simeq \frac{\sqrt{\varepsilon}(1 + \sqrt{1 - \alpha^2\varepsilon})(\sqrt{1 + \alpha} - \sqrt{1 - \alpha})}{1 + (1 - \alpha^2)\varepsilon^2}. \tag{2}$$

The estimation of the values of α for NiMnSb and PtMnSb give 0.04 and 0.12, respectively, i.e. in any case $\alpha \ll 1$. The position of the maximum in $\theta(\varepsilon)$ is determined by the variation in ε with regard to the smallness of α: $\varepsilon \sim 1/\sqrt{1 - \alpha^2}$). So the theoretical limit

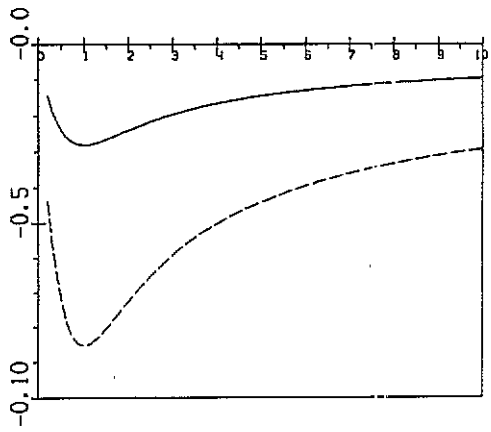

Figure 8. The Kerr angle model dependence versus dielectric function $\mathrm{Im}[\varepsilon_{xx}(\omega)]$ near the plasma resonance. The cases with $\alpha = 0.04$ (——) and $\alpha = 0.12$ (– – – –) may be conditionally ascribed to NiMnSb and PtMnSb, respectively.

of the Kerr angle at the plasma frequency is determined by the ratio of the non-diagonal to the diagonal components: $\max[\theta(\omega \sim \omega_p)] \sim -\alpha/\sqrt{2}$ provided that $\mathrm{Im}[\varepsilon_{xx}(\omega \sim \omega_p)] \sim 1/\sqrt{1-\alpha^2} \sim 1$. Figure 8 schematically shows the $\mathrm{Im}(\varepsilon_{xx})$-dependence of θ at various α. Usually the occurrence of the plasma threshold is accompanied by strong one-electron transitions at the energies near to $\hbar\omega_p$. In the vicinity of $\hbar\omega_p$ let us denote $\max[\varepsilon(\omega)]$ by ε'. At energies near but not equal to $\hbar\omega_p$, $\theta' \sim -\alpha/\sqrt{2\varepsilon'}$. Therefore the maximum enhancement $\max[\theta(\omega \simeq \omega_p)]/\theta'$ of MOKE through the plasma resonance is estimated as $\sqrt{\varepsilon'}$.

Since $\mathrm{Im}[\varepsilon_{xy}(\omega)] \sim \alpha'\{\mathrm{Re}[\varepsilon^{\uparrow}_{xx}(\omega) - \mathrm{Re}[\varepsilon^{\downarrow}_{xx}(\omega)]\}$, in order for the outlined effect to be realized, it is essential that one of the components $\mathrm{Re}[\varepsilon^{\uparrow}_{xx}(\omega)]$ or $\mathrm{Re}[\varepsilon^{\downarrow}_{xx}(\omega)]$ should be small compared with others in the neighbourhood of the plasma frequency ω_p. So the compounds with 100% spin polarization could serve as a system in which the enhancement of MOKE was obtained at $\omega \sim \omega_p$, because in this case $\mathrm{Im}[\varepsilon_{xy}(\omega)] \sim \alpha'\,\mathrm{Re}[\varepsilon^{\uparrow}_{xx}(\omega)]$ or $\mathrm{Im}[\varepsilon_{xy}(\omega)] \sim \alpha'\,\mathrm{Re}[\varepsilon^{\downarrow}_{xx}(\omega)]$ and the additional smallness of $\mathrm{Im}[\varepsilon_{xy}(\omega)]$ associated with the difference $\mathrm{Re}[\varepsilon^{\uparrow}_{xx}(\omega)] - \mathrm{Re}[\varepsilon^{\downarrow}_{xx}(\omega)]$ disappears. The compounds under consideration could be such systems provided that the value of the optical gap $\Delta^{\downarrow}_{opt}$ in the spin-down subband is greater than $\hbar\omega_p$, i.e. if the interband spin-down transitions start at energies $\hbar\omega > \hbar\omega_p$.

The value of the optical gap $\Delta^{\downarrow}_{opt}$ is calculated to be about 1.0 eV for NiMnSb and PtMnSb while calculations of the characteristic loss energy functions $L(\omega) = -\mathrm{Im}\,\varepsilon^{-1}_{xx}(\omega)$ yield the plasma energy $\hbar\omega_p \sim 1.5$ eV for both compounds (see figure 9, where $\mathrm{Im}\,\varepsilon_{xx}(\omega)$, $\mathrm{Re}\,\varepsilon_{xx}(\omega)$, the reflectivity coefficient $R(\omega)$ and $L(\omega)$ for PtMnSb are presented), i.e. $\Delta^{\downarrow}_{opt} < \hbar\omega_p$. This is mainly responsible for the lack of an enhancement of MOKE at $\omega \sim \omega_p$ in our calculations. We have drawn the conclusion that the calculations of the actual one-electron excitations would require an essential improvement.

It may be supposed that in NiMnSb and PtMnSb there is an enhancement of MOKE at $\omega \sim \omega_p$ owing to the spin-down gap in band spectrum and to the small size of the intraband contribution to the conductivity. At the same time in PtMnSn this effect is suppressed due to the relatively large value of the intraband contributions.

In US a completely different mechanism forms optics and magneto-optics at the energy where the maximum MOKE occurs ($\hbar\omega \sim 1.6$ eV). There are the U f states both with the spin-up and spin-down near E_F. As was mentioned earlier, interband transitions, appearing due to the hybridization initiated by the SOI, with simultaneous participation

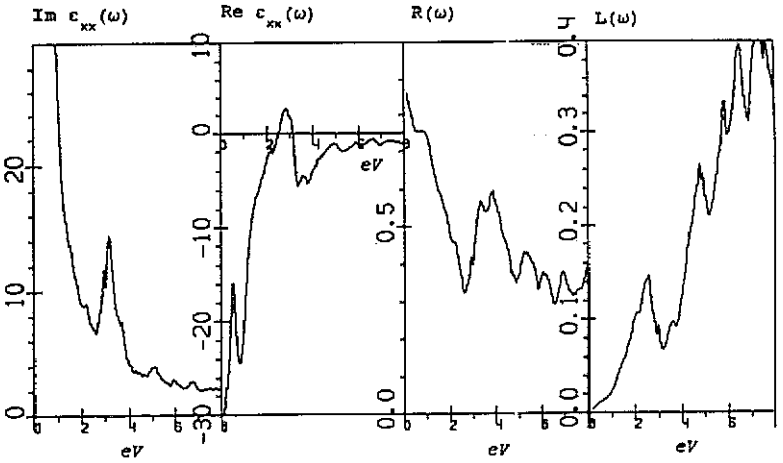

Figure 9. Energy dependences of $\mathrm{Im}[\varepsilon_{xx}(\omega)]$, $\mathrm{Re}[\varepsilon_{xx}(\omega)]$ $R(\omega)$ and $L(\omega)$ for PtMnSb.

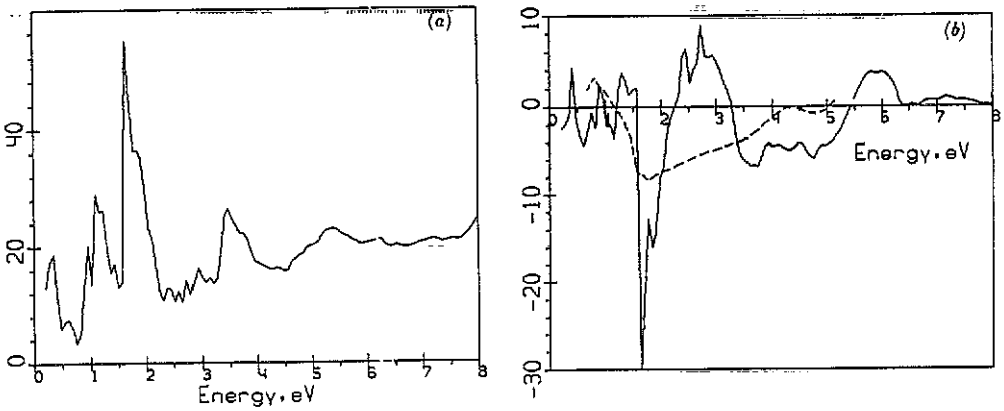

Figure 10. Optical characteristics of US: (*a*) $\mathrm{Re}[\sigma_{xx}(\omega)]$; (*b*) $\mathrm{Im}[\sigma_{xy}(\omega)]$ (– – – –, experiment (Reim 1986)). All values are in units of $10^{14}\ \mathrm{s}^{-1}$.

of spin-up and spin-down electrons lead to the peaks in Re σ_{xx} and Im σ_{xy} at the energy $\hbar\omega \sim 2\bar{\xi}$ or more precisely at $\hbar\omega \sim 2\sqrt{|\bar{\xi}|^2 + \Delta_{xc}^2}$. Figure 10 shows that Re σ_{xx} and Im σ_{xy} have sharp peaks at the energy $\hbar\omega \sim 1.6$ eV (we do not know the experimental data for Re $\sigma_{xx}(\omega)$ in the ferromagnetic phase of US). These peculiarities are formed by the U d → f transitions. According to our calculations, the maximum Kerr angle is found at the energy $\hbar\omega \sim 1.6$ eV due to the above-mentioned SOI effect, thus the result corresponds closely to the experiment (Reim 1986), even though the calculated Kerr angle is several times greater than the experimental one. The ratio of the non-diagonal component to the diagonal one is about $\bar{\xi}/\Delta\bar{E} \sim 1$. Of course, when the ratio Im σ_{xy}/Re σ_{xx} is defined, we should take into account not only the mentioned contribution into the conductivity tensor, but also the contribution into the tensor initiated by the usual interband transitions between states with similar spin projections.

5. Conclusions

As the calculations showed, 100% spin polarization at the Fermi level and large values of the magnetic moment and SOI do not assure in themselves a large MOKE. The analysis of the electron spectra and optical properties in NiMnSb, PtMnSb and PtMnSn indicates that the amplitude of the non-diagonal component of the conductivity tensor $\mathrm{Im}[\sigma_{xy}(\omega)]$ is determined in particular by the SOI value on the Ni(Pt) atoms. At the same time, $\mathrm{Im}[\sigma_{xy}(\omega)]$ is due to the difference between transitions with opposite spins or equivalently the difference between spin-up and spin-down DOSs at a given energy. The almost non-existence of the MOKE in our calculations at those energies (1.5 eV) where the experimental maxima of the MOKE are observed seems to be caused by the incorrect value of the optical spin-down gap (1.0 eV) which is obtained in the LSD theory. In comparison with the above-mentioned energies (1.5 eV), it leads to almost complete compensation of the transitions with the opposite spins. The analysis shows that, even at a comparatively small value of $\mathrm{Im}[\sigma_{xy}(\omega)]$ the amplitude of the MOKE can increase several times if the plasma resonance exists. In this respect, NiMnSb and PtMnSb, in which the intraband contribution at an energy of 1.5 eV is much less than in PtMnSn (the MOKE amplitude in PtMnSn is even weaker than in NiMnSb, although the SOI value is several times higher), are more suitable for plasma resonance.

In contrast with the HMFS, in which the enhancement of the MOKE at comparatively small values of components of the conductivity tensor is possible, the example of a compound such as US, which is not a HMF, can be given. The following circumstance, i.e. the lack of a gap in both spin subbands and the existence of intersections and proximity regions of non-relativistic bands with opposite spins, is the condition for the realization of the interband mechanism, leading to the sharp enhancement of the MOKE at energies near $\hbar\omega \simeq 2\sqrt{|\xi|^2 + \Delta_{xc}^2}$ (both ξ and Δ_{xc} are related to U atoms). This sharp enhancement is initiated by the abnormal contributions to the conductivity tensor.

Acknowledgments

The authors are grateful to Dr V V Losyakov and Dr Yu A Uspenskii for helpful discussions.

References

Andersen O K 1975 *Phys. Rev.* B **12** 3060
Argyres P N 1955 *Phys. Rev.* **97** 334
de Groot R A, Mueller F M, van Engen P G and Buschow K H J 1983 *Phys. Rev. Lett.* **50** 2024
de Groot R A, van der Kraan A M and Buschow K H J 1986 *J. Magn. Magn. Mater.* **61** 330
Feil H and Haas C 1987 *Phys. Rev. Lett.* **58** 65
Gunnarsson O and Lundqvist B I 1976 *Phys. Rev.* B **13** 4274
Halilov S V and Uspenski Yu A 1988 *Fiz. Metall. Metalloved.* **66** 1097
—— 1990 *J. Phys.: Condens. Matter* **2** 6137
Itzykson C and Zuber J-B 1980 *Quantum Field Theory* (New York: McGraw-Hill)
Janak J F, Moruzzi V L and Williams A R 1975 *Phys. Rev.* B **12** 1257
Kleiner W H 1966 *Phys. Rev.* **142** 318
Kubo R 1957 *J. Phys. Soc. Japan* **12** 570
Kuebler J 1984 *Physica* B **127** 207
Kulatov E and Mazin I I 1990 *J. Phys.: Condens. Matter* **2** 343

Otto M J H, van Woerden R A M, van der Valk P J, Wijngaard J H, van Bruggen C F and Haas C 1989 *J. Phys.: Condens. Matter* **1** 2351
Reim W 1986 *J. Magn. Magn. Mater.* **58** 1
Schwarz K 1986 *J. Phys. F: Met. Phys.* **16** L211
Uspenski Yu A, Maksimov E G, Mazin I I and Rashkeev S N 1983 *Z. Phys.* B **53** 263
van der Heide P A M, Baelde W, de Groot R A, de Vroomen A R, van Engen P G and Buschow K H J 1985 *J. Phys. F: Met. Phys.* **15** L75
van Engen P G, Buschow K H J, Jongenbreur R and Erman M 1983 *Appl. Phys. Lett.* **42** 202
von Barth U and Hedin L 1972 *J. Phys. C: Solid State Phys.* **5** 1629
Vosko S H, Wilk L and Nussair M 1980 *Can. J. Phys.* **58** 1200
Wijngaard J H, Haas C and de Groot R A 1989 *Phys. Rev.* B **40** 9318
Yanase A and Siratori K 1984 *J. Phys. Soc. Japan* **33** 312